CS231n Project: Particle Identification and Energy Reconstruction in Calorimeter Readout Using dSiPM

Liangyu Wu Qihua Wang Bo Liu
Stanford University
Stanford, CA 94305, USA
{liangyu5, qihuaw, boliu02}@stanford.edu

Abstract

State-of-the-art calorimeter designs enable increasingly precise particle energy measurements in high-energy physics experiments. Using Geant4-based simulations and assuming signal readout with advanced dSiPM technology, we investigated particle identification and energy reconstruction using the Convolutional Neural Network (CNN). Our findings demonstrate that deep neural networks have the potential to achieve superior energy resolution measurements and perform particle classification with exceptional accuracy. Furthermore, we observed that incorporating finer timing information can further enhance our network's hadronic energy resolution capabilities.

1. Introduction

1.1. Advances in Calorimetry for Particle Physics

Precision energy measurement is fundamental to modern high-energy physics research. Calorimeters serve as sophisticated detection systems that measure energy deposition when particles interact with detector material. These interactions produce characteristic shower patterns through electromagnetic and hadronic processes, yielding signals that contain crucial information about particle properties. Various specialized calorimeter designs have been developed to meet specific experimental needs, including electromagnetic calorimeters, hadronic calorimeters, and recently dual-readout calorimeters, each optimized for different particle types and energy regimes.

Despite significant technological advancements, conventional calorimetric data processing follows a largely unchanged paradigm: analog signal collection, waveform digitization, and subsequent offline reconstruction. This established methodology, while robust, likely underutilizes the wealth of information embedded within particle shower development. For example, the dual-readout approach [11] represented a conceptual breakthrough by separately measuring electromagnetic and non-electromagnetic shower components to improve energy resolution. However, even these advanced techniques have not yet achieved theoretical resolution limits, suggesting that substantial information—perhaps contained in the fine-grained spatial and temporal structure of energy deposits—remains unexploited by traditional reconstruction methods.

1.2. Neural Networks for Calorimeter Analysis

Machine learning techniques have emerged as powerful tools for calorimeter data analysis. Deep neural networks, specifically CNNs and GNNs, excel at extracting complex patterns from high-dimensional data. Recent studies have demonstrated that these approaches can achieve superior performance in calorimetric energy reconstruction [2, 12] compared to traditional methods.

In this study, we apply deep learning techniques to analyze spatial energy distribution patterns in calorimeters, aiming to improve both energy reconstruction precision and particle identification capabilities. Our approach is enhanced by recent advances in detector technology, particularly the digital Silicon Photomultiplier (dSiPM) [7], which provides direct access to photon count distributions without intermediate waveform processing. This combination of advanced readout technology and neural network analysis shows significant promise for enhancing the performance of calorimetric measurements in future particle physics experiments.

1.3. Network Inputs and Outputs

We will use simulation results from the calorimeter as our input data. These data consist of time-evolving 2D distributions representing photon deposition patterns within the detector as particles enter and produce showers. By capturing shower development across multiple time frames, we obtain not just a single image but a sequence of frames showing the temporal evolution of each shower event. Assuming the use of dSiPM as the photon detection endpoint, we record energy deposition distributions as photon counts

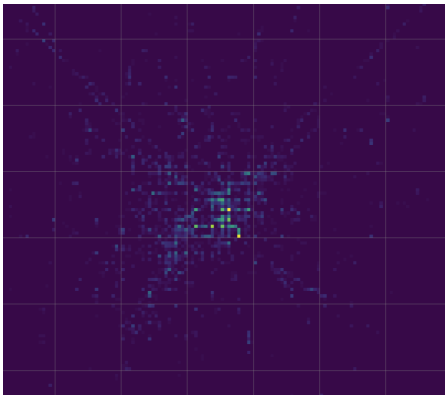

Figure 1. 90 GeV π^- shower image across the full detector cross-section. The light dots represent the number of photons collected.

across each pixel at different time intervals. The 2D image shown in Figure 1 represents the distribution of photon counts from a 90 GeV hadronic shower within the calorimeter at a specific time slice. The input data will include various energy ranges (1-100 GeV) and particle types, provided we have a sufficiently large dataset. In addition to the multi-frame 2D image input, we incorporate an auxiliary parameter, E_{sum}, which represents the total energy deposition summed across all pixels in the event. This provides complementary energy information after the 2D image sequence has been normalized. We will feed this time-dependent shower data into our model with the expectation of producing two outputs:

- The type of incoming particle: e^-, π^-, etc.
- The energy of the incoming particle

2. Current Approaches in Calorimetric Energy Reconstruction

2.1. Particle Flow Analysis

One significant approach to enhancing energy resolution in calorimetry is Particle Flow Analysis (PFA). As comprehensively reviewed by this paper [15], PFA combines calorimeter measurements with magnetic tracker data to reconstruct jets. The core principle involves using tracker information to measure charged particle momenta while relying on calorimeter data for neutral particle energy measurements, theoretically leveraging the superior momentum resolution of tracking detectors.

Despite its theoretical advantages, PFA faces substantial practical challenges. The primary difficulty lies in avoiding double-counting of energy—charged particles measured by the tracker also deposit energy in the calorimeter, requiring sophisticated algorithms to disentangle these contributions. Additionally, errors in track-cluster matching can propagate through the reconstruction chain, either removing valid energy deposits or including spurious ones, ultimately degrading the reliability of the final energy measurements.

2.2. Dual-Readout Calorimetry

In high-energy physics experiments, achieving optimal energy resolution remains a significant challenge, particularly for hadrons at lower energies. Dual-readout calorimetry has emerged as one of the most promising approaches to address this challenge. The fundamental principle of dual-readout calorimeters, as described by Lee et al. [11] and Pareti et al. [14], involves utilizing two distinct signal readout channels: one sensitive exclusively to energy deposited by relativistic particles in the shower, and another responsive to energy depositions from all charged particles within the shower. This approach enables the disentanglement of electromagnetic and hadronic components of particle showers, theoretically improving energy resolution.

This work [6] demonstrated through Geant4 standalone simulations that dual-readout techniques can yield significant improvements in energy resolution for certain calorimeter materials, such as $PbWO_4$. However, their results also revealed an important limitation: the performance enhancements were inconsistent across different detector materials and configurations. Some of these questions have been answered in this paper [8], but this inconsistency still suggests that while detector design advancements have been made, we have not yet fully exploited all available information from particle showers to achieve optimal resolution improvements.

2.3. Neural Network Applications

Given the limitations of both particle flow analysis and dual-readout techniques, researchers have increasingly turned to machine learning approaches to extract maximum information from calorimeter signals. Neural networks, with their capacity to identify complex patterns in high-dimensional data, offer a promising alternative to traditional reconstruction methods. Several studies have explored this direction, applying various deep learning architectures to calorimeter data. Some early successes [4] have been demonstrated using deep neural networks for jet classification tasks, while Komiske et al. [10] pioneered the application of convolutional neural networks to jet images. Carminati et al. [5] further advanced simulation techniques using adversarial generative networks. In the domain of calorimeter-based particle identification, convolutional neural networks were applied to improve classification accuracy [3] in neutrino experiments.

More specifically in the realm of energy reconstruction, several works [2, 13] have demonstrated promising results applying neural networks to particle energy reconstruction. Also the work from [12] presents the energy and angle re-

gression with the help of GNNs. These studies primarily relied on comprehensive 3D shower information available in simulations, using spatial distribution patterns to train neural networks for prediction. While this approach provides excellent proof-of-concept validation, acquiring such detailed shower information in complex experimental environments presents significant practical challenges.

Our research diverges from these previous works by focusing exclusively on signals obtained from silicon sensors at the final readout stage of the calorimeter. By utilizing both the spatial and temporal distribution of these signals, our approach offers greater practicality and comparative relevance to experimental conditions. This methodology bridges the gap between simulation-based studies and experimental implementation, has great potential to achieve optimal energy resolution while maintaining robust performance across different particle types and energy ranges.

3. Methodology and Dataset

3.1. Dataset Generation and Characteristics

Our dataset is derived from standalone detector simulations implemented using Geant4 [1], a toolkit widely used in high-energy physics for modeling particle interactions with matter. The simulation code [9] implements the HG-DREAM calorimeter geometry and simulates energy deposition processes of various particles within the detector. This simulation generates ROOT files containing comprehensive information about particle interactions, which we subsequently process and convert to HDF5 format for efficient deep learning model training.

The dataset consists of 8,000 simulated events distributed among electrons and pions with energies ranging from 1 to 100 GeV. Additionally, we prepared a separate test dataset containing 1,000 events for each particle type to evaluate model performance across different energy regimes. The detailed breakdown of these datasets is presented in Table 3.1. We partition this dataset into training, validation, and test sets using a 70%/20%/10% split, resulting in approximately 5,600 training events, 1,600 validation events, and 8,800 test events.

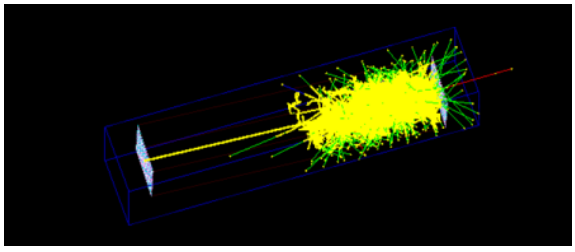

Figure 2. Event display showing the shower pattern of a 50 GeV π^- entering the detector at normal incidence. The yellow-colored points represent energy depositions within the detector volume.

Each event in our dataset represents the spatial and temporal distribution of photons detected by dSiPMs at the end of optical fibers. Figure 2 illustrates a typical event display showing the shower pattern produced by a 50 GeV π^- entering the detector at normal incidence. The shower development leads to energy depositions that generate photons, which propagate through the fibers and are ultimately detected by the dSiPMs at the detector periphery.

The data for each event is structured as a 2D histogram with dimensions 159×139, where each pixel corresponds to a 0.4 cm × 0.4 cm area in the detector, matching the cross-sectional size of a rod containing four Cherenkov fibers and three scintillation fibers. Figure 3 shows the Cherenkov photon distributions in one single rod, where the four circles stand for the arrangement of the Cherenkov fibers. This spatial resolution captures the detailed structure of particle showers while maintaining a computationally manageable input size for our neural network.

Table 1. Summary of the final dataset

Particle Type	Number of Events	Train / Val / Test
1-100 GeV e^-	4000	2800 / 800 / 400
1-100 GeV π^-	4000	2800 / 800 / 400
10, 30, 50, 90 GeV e^-	1000	0 / 0 / 1000
10, 30, 50, 90 GeV π^-	1000	0 / 0 / 1000

Figure 3. Photon occupancy in a single rod. The color of each pixel stands for the number of photons received in that channel.

A unique aspect of our dataset is the temporal dimension—each event includes multiple time slices capturing the shower development over time. This temporal information provides crucial distinguishing features between particle types, as particles and anti-particles exhibit characteristically different shower development patterns over time, which is also true for leptons and hadrons.

3.2. Data Preprocessing

Prior to model training, we apply several preprocessing steps to enhance learning efficiency:

1. **Energy Sum Normalization**: The total energy sum for each event is standardized using:

$$\tilde{E}_{\text{sum}} = \frac{E_{\text{sum}} - \mu_{E_{\text{sum}}}}{\sigma_{E_{\text{sum}}}} \tag{1}$$

where $\mu_{E_{\text{sum}}}$ and $\sigma_{E_{\text{sum}}}$ are the mean and standard deviation computed from the training set.

2. **Particle Type Encoding**: Particle types are one-hot encoded for classification purposes.

3. **Energy Scaling**: True particle energies are scaled to GeV (divided by 1000 from the original MeV values) to improve numerical stability during training.

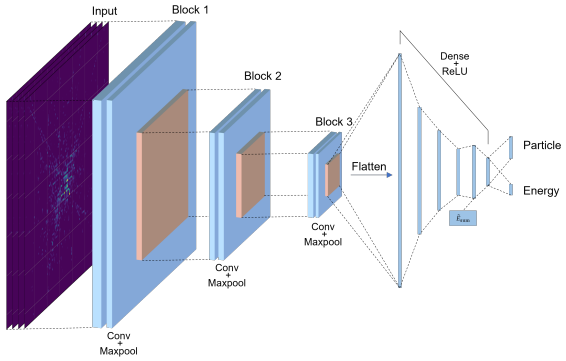

Figure 4. CNN architecture for particle ID and energy regression.

3.3. Neural Network Architecture

We implement a convolutional neural network architecture 4 designed to effectively process both spatial and temporal features of calorimeter data. Our network input can be formally represented as a 4-dimensional tensor $X \in \mathbb{R}^{N\times H\times W\times C}$, where N is the batch size, $H = 159$ and $W = 139$ are the spatial dimensions, and C represents the selected time slices (we are starting from $C = 12$, i.e. about 1.0 ns time steps).

The core architecture consists of three convolutional blocks with the following structure:

$$\text{Block 1}: \begin{cases} \text{Conv2D}(5\times 5, 64) \to \text{ReLU} \to \text{BatchNorm} \\ \text{Conv2D}(3\times 3, 32) \to \text{ReLU} \to \text{MaxPool}(2\times 2) \end{cases}$$

$$\text{Block 2}: \begin{cases} \text{Conv2D}(3\times 3, 32) \to \text{ReLU} \to \text{BatchNorm} \\ \text{Conv2D}(3\times 3, 32) \to \text{ReLU} \to \text{MaxPool}(2\times 2) \end{cases}$$

$$\text{Block 3}: \begin{cases} \text{Conv2D}(3\times 3, 32) \to \text{ReLU} \to \text{BatchNorm} \\ \text{Conv2D}(3\times 3, 16) \to \text{ReLU} \to \text{MaxPool}(2\times 2) \end{cases}$$

These convolutional layers progressively extract hierarchical features from the input data. The first layer uses larger 5×5 filters to capture broader spatial patterns, while subsequent layers use 3×3 filters to extract more refined shower features. Batch normalization layers help stabilize training by normalizing activations, while max-pooling operations reduce spatial dimensions and provide translation invariance.

Following the convolutional blocks, the network continues with:

$$\begin{aligned} \text{Flatten} &\to \text{Dense}(512) \to \text{ReLU} \to \text{Dropout}(0.2) \\ &\to \text{Dense}(128) \to \text{ReLU} \to \text{Dropout}(0.2) \\ &\to \text{Dense}(64) \to \text{ReLU} \to \text{Dropout}(0.2) \end{aligned}$$

We also incorporate the total energy sum as an additional feature in our architecture. We concatenate the learned features with the normalized energy sum before the final output layers:

$$\mathbf{h}_{\text{combined}} = [\mathbf{h}_{\text{CNN}}, \tilde{E}_{\text{sum}}] \to \text{Dense}(32) \to \text{ReLU}$$

Finally, we produce two outputs:

$$\begin{aligned} \mathbf{y}_{\text{particle}} &= \text{Dense}(4/2) \to \text{Softmax} \\ \mathbf{y}_{\text{energy}} &= \text{Dense}(1) \end{aligned}$$

where $\mathbf{y}_{\text{particle}}$ represents the probability distribution over particle types (electron vs. pion), and $\mathbf{y}_{\text{energy}}$ is the predicted energy of the incident particle. There could be 4 or 2 neurons in the dense layer for $\mathbf{y}_{\text{particle}}$ depending on how many different particles we hope the model to distinguish.

3.4. Training Methodology

We formulate our problem as a multi-task learning objective combining particle identification (classification) and energy reconstruction (regression). The combined loss function is:

$$\mathcal{L}_{\text{total}} = \lambda_1 \mathcal{L}_{\text{particle}} + \lambda_2 \mathcal{L}_{\text{energy}} \tag{2}$$

where λ_1 and λ_2 are weighting coefficients that balance the contribution of each task. For particle identification, we use categorical cross-entropy loss:

$$\mathcal{L}_{\text{particle}} = -\sum_{i=1}^{N}\sum_{c=1}^{2} y_{i,c}\log(\hat{y}_{i,c}) \tag{3}$$

For energy reconstruction, we employ mean squared logarithmic error (MSLE):

$$\mathcal{L}_{\text{energy}} = \frac{1}{N}\sum_{i=1}^{N}(\log(1+y_i) - \log(1+\hat{y}_i))^2 \tag{4}$$

This logarithmic transformation helps balance the importance of relative errors across the wide range of particle energies (1-100 GeV) in our dataset.

Figure 5 shows a visualization of the six selected time channels (about 2 ns time steps) for representative electron and pion events. The distinctive spatial patterns and temporal evolution characteristics provide rich information for our neural network to differentiate between particle types.

Our implementation uses TensorFlow 2.x with the Keras API, building the entire model architecture and training pipeline from scratch without relying on pre-existing specialized code bases.

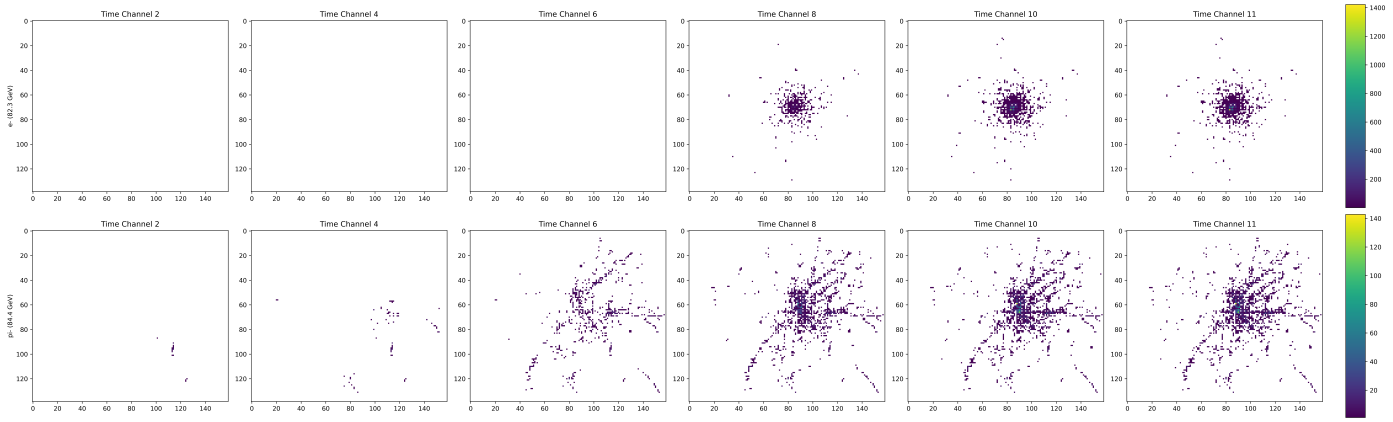

Figure 5. Temporal evolution of particle showers in the calorimeter. Top row: 82.3 GeV electron shower development. Bottom row: 84.4 GeV pion shower development. Each column represents a time slice approximately 2 ns apart.

4. Experiments and Results

4.1. Experimental Setup and Hyperparameters

We train the model using the Adam optimizer with a learning rate of 10^{-4} and a batch size of 256. The relatively low learning rate was chosen to prevent oscillations in the loss landscape given the complexity of our multi-task objective. To prevent overfitting, we implement early stopping based on validation loss and use dropout layers with a rate of 0.2. Our training procedure includes an iterative approach allowing for multiple training rounds, which helps escape local minima. The loss function weights ($\lambda_1 = 1.0$ and $\lambda_2 = 10.0$) were determined through cross-validation experiments, placing greater emphasis on the energy reconstruction task since we found that it is much harder for the model to perform better in the energy reconstruction task. This weighting scheme effectively balances the numerical scales of the categorical cross-entropy and mean squared logarithmic error components.

To prevent overfitting, we implemented several regularization strategies. Dropout layers with a rate of 0.2 were inserted after dense layers, randomly deactivating 20% of neurons during training to reduce co-adaptation. Batch normalization was applied after convolutional layers to stabilize training and mitigate internal covariate shift. Early stopping monitored validation loss with a patience of 10 epochs, halting training when no improvement was observed and restoring the best-performing model weights. Each training run taking approximately 1.5 hours to complete. The final best model were selected based on performance across 10 runs submitted on the cluster. The loss curve shows the good training performance of our model after 30 epochs.

When training with finer temporal granularity (larger C values), we encountered significant system memory constraints due to the increased dataset size. To address this limitation, we implemented an incremental training strategy using sequential data chunks. Instead of loading the entire dataset into memory at once, we randomly sampled 250 events from each particle type per iteration, trained with a reduced batch size, and saved the resulting model. This model then served as the initialization point for training on the next data chunk, creating an iterative refinement process. This approach effectively transforms the training procedure into a form of curriculum learning, where the model progressively improves its representations while maintaining memory efficiency.

4.2. Evaluation Metrics

4.2.1 Particle Identification Metrics

For the particle classification task, we report:

- **Accuracy**: The proportion of correctly classified particles, defined as:

$$\text{Accuracy} = \frac{\text{Number of correctly classified particles}}{\text{Total number of particles}} \tag{5}$$

- **Confusion Matrix**: A table showing the distribution of predicted vs. true particle types, providing insight into classification errors.

- **ROC Curve**: The Receiver Operating Characteristic curve plotting the true positive rate against the false positive rate at various threshold settings, with the Area Under the Curve (AUC) quantifying the overall classification performance independent of any specific threshold.

4.2.2 Energy Reconstruction Metrics

For the regression task of energy reconstruction, we use:

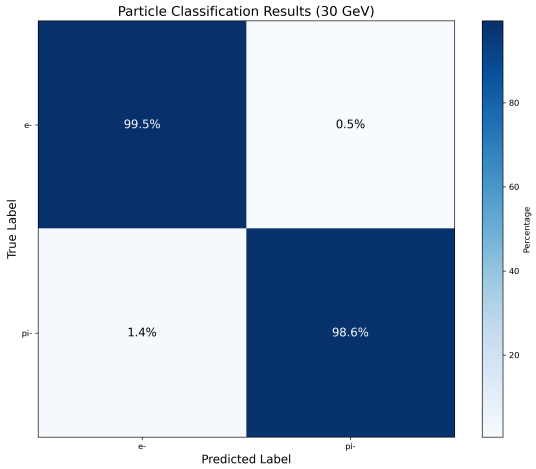

Figure 6. Confusion matrices showing particle identification performance for 30 GeV electrons and pions. Both particle types are classified with accuracy exceeding 98.5%.

- **Mean Absolute Error (MAE)**: The average absolute difference between predicted and true energies:

$$\text{MAE} = \frac{1}{N}\sum_{i=1}^{N}|y_i - \hat{y}_i| \tag{6}$$

- **Energy Resolution**: Defined as σ_E/E, where σ_E is the standard deviation of the reconstructed energy distribution for events with true energy E:

$$\text{Resolution} = \frac{\sigma_E}{E} = \frac{\sqrt{\frac{1}{N}\sum_{i=1}^{N}(y_i - \hat{y}_i)^2}}{E} \tag{7}$$

This metric is particularly important in calorimetry, as it characterizes the detector's ability to distinguish particles with similar energies.

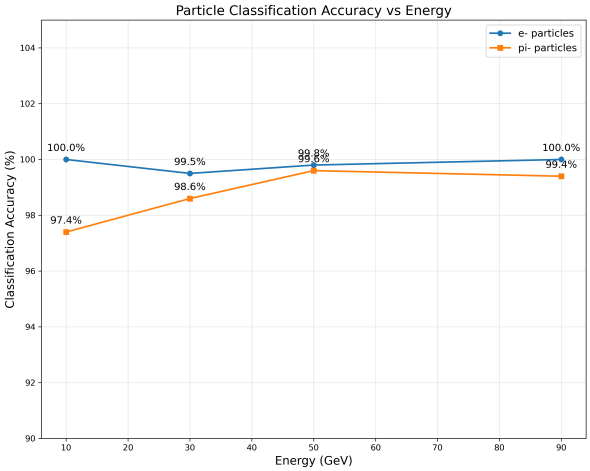

Figure 7. Particle identification accuracy across different energy levels.

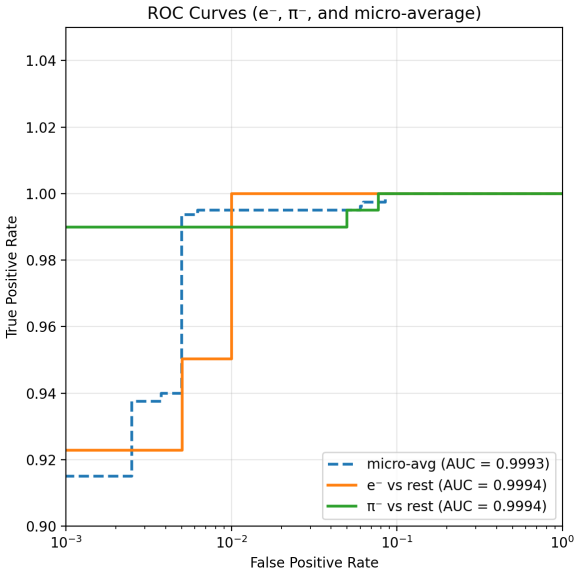

Figure 8. ROC curve for the model.

- **Energy Response**: The relationship between mean reconstructed energy and true energy, ideally following a horizontal line with height 1.0.

4.3. Model Performance

4.3.1 Particle Identification

Our CNN-based model demonstrates exceptional performance in particle identification tasks. Figure 6 presents confusion matrices for 30 GeV electrons and pions, showing classification accuracies exceeding 98.5% for both particle types. This high accuracy underscores the model's ability to

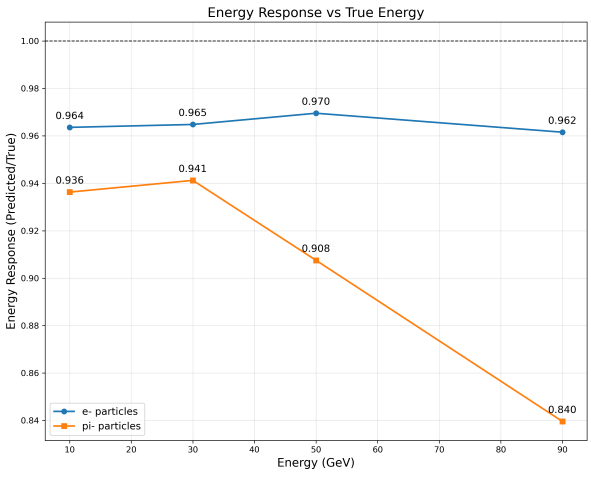

Figure 9. Ratio of reconstructed to true energy across different energy levels for electrons and pions.

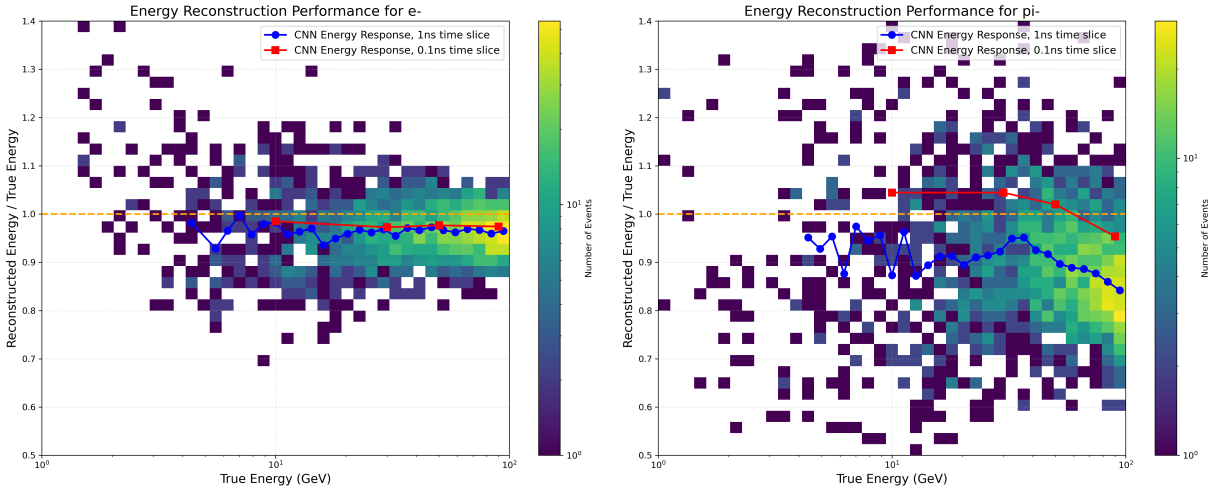

Figure 10. Energy response as a function of true particle energy for electrons (left) and pions (right). Color intensity indicates event density, while the blue line shows the mean response at each energy level in 1 ns time slices and red for 0.1 ns.

effectively learn discriminative features from the calorimeter information.

The model's identification capability remains robust across various energy levels, as demonstrated in Figure 7. For each energy level, we tested the model on 1,000 events per particle type, consistently achieving classification accuracies above 97%. Notably, electrons are identified with higher accuracy compared to pions across all energy ranges. This performance differential can be attributed to the more concentrated EM shower patterns produced by electrons, compared to the more variable hadronic showers of pions.

The ROC curve in Figure 8 shows that the model can achieve a true positive rate of more than 0.9 with a false positive rate of less than 10^{-3}. And the AUC can reach the 0.9994 level for e^-, π^- and microaverage of both.

4.3.2 Particle Energy Reconstruction

Figure 9 presents the ratio of mean reconstructed energy to true energy for electrons and pions across various energy levels. Both types of particles show reconstruction accuracy that exceeds 84% throughout the energy spectrum tested. In particular, electrons show consistent reconstruction performance across the entire 1-100 GeV range due to their predictable electromagnetic shower characteristics. Pions, however, exhibit declining reconstruction accuracy above 70 GeV, likely due to "punch-through" effects where portions of high-energy hadronic showers escape the detector volume rather than any model deficiency.

Figure 10 presents the energy response (defined as the ratio of reconstructed to true energy) as a function of true particle energy. This visualization reveals important characteristics of our model's energy reconstruction capabilities across the full energy spectrum. The plots demonstrate a clear trend where reconstruction efficiency improves with increasing particle energy for both particle types, stabilizing at higher energies. For pions, we observe a decline in the mean response curve at energies above approximately 70 GeV, confirming our earlier hypothesis about detector punch-through effects. When we reduced the time interval between image frames from 1 ns to 0.1 ns, the data shown in red demonstrated a slight improvement for electrons and a more pronounced enhancement for pions.

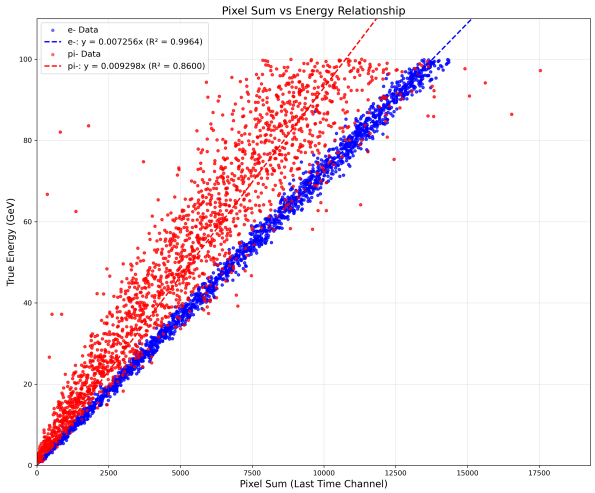

Figure 11. Linear relationship between the total pixel sum in the final time channel and true particle energy.

4.3.3 Energy Reconstruction with Linear Calibration

Given that the energy deposited by particles is proportional to the number of photons produced in the calorimeter, we investigated a direct calibration approach as a benchmark

method. Figure 11 shows the linear relationship between true energy and the sum of pixel values in the final time channel for both electrons and pions. The strong linear correlation observed in this plot (with $R^2 = 0.9964$ for electrons and $R^2 = 0.8600$ for pions) suggests that a simple linear calibration could provide a reasonable first-order energy estimate. We leveraged this relationship to implement a direct energy reconstruction method by multiplying the sum of pixel values by the corresponding calibration factor for each particle type. This straightforward calibration serves as a baseline for evaluating our neural network approach, representing the most direct way to estimate particle energy from detected photon counts with minimal signal processing in actual experiments.

4.3.4 Comparison of Reconstruction Methods

To evaluate the effectiveness of our neural network approach, we compared the energy resolution achieved by our CNN model against the linear calibration method across different energy levels. Figure 12 presents this comparison for both electrons and pions. This performance difference aligns with established calorimetry principles, where EM showers typically yield better energy resolution. As expected, both methods show improved energy resolution with increasing particle energy, following the characteristic $1/\sqrt{E}$ scaling behavior typical of calorimeter systems.

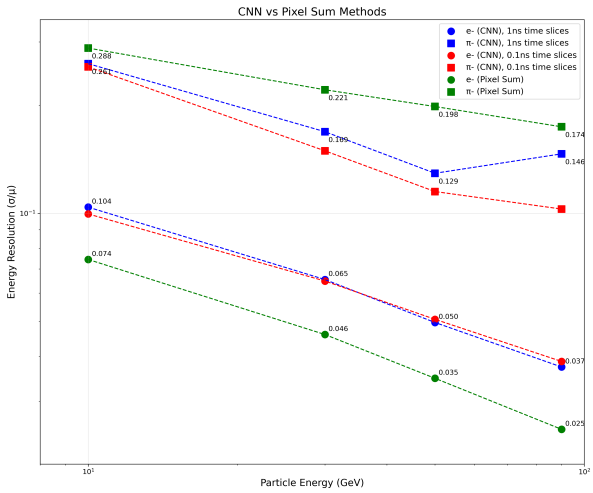

Figure 12. Energy resolution as a function of particle energy for both CNN and linear calibration methods.

The comparison reveals an interesting pattern: for electrons, the linear calibration method actually shows slightly better resolution than our CNN approach, suggesting room for improvement in our model for electromagnetic showers. However, this is acceptable as electron energy resolution is generally not the most challenging aspect of calorimetry due to the more predictable nature of EM showers.

Our primary focus was improving hadronic energy resolution, where traditional calorimetry techniques often struggle. In this regard, the CNN method demonstrates significantly superior performance compared to the linear calibration approach across all energy levels for pions. This improvement is particularly pronounced at lower energies, where hadronic shower fluctuations are more significant and the complex pattern recognition capabilities of neural networks provide greater advantage. The enhanced performance for pions indicates that our model successfully extracts additional information from the spatial and temporal distribution of hadronic shower development beyond what is captured by the simple sum of detected photons. Additionally, the figure also indicates that using more finely divided time steps can further improve hadronic energy resolution.

5. Conclusion and Future Work

This study demonstrates the effectiveness of CNNs in extracting information from calorimeter data for particle identification and energy reconstruction. Our approach achieves high accuracy in distinguishing between electrons and pions while simultaneously providing precise energy measurements across a wide energy range. Our results indicate that the integration of temporal information significantly enhances model performance, particularly for energy reconstruction at lower energies where traditional calorimetry techniques often struggle. The network effectively learns distinctive shower development patterns that characterize different particle types, providing a powerful complement to existing dual-readout calorimetry approaches. Furthermore, our direct utilization of detector signals eliminates the need for complex intermediate processing steps, offering a more streamlined analysis pipeline for future experiments.

For future work, we plan to enhance our simulation with more accurate modeling of scintillation light production and propagation, which would enable direct comparison with state-of-the-art energy resolution benchmarks from traditional reconstruction methods. Additionally, we aim to explore finer temporal resolution in our detector readout, potentially reaching the 10 ps. Such ultra-high time resolution would provide even more detailed information about shower development dynamics, potentially revealing subtle features that could further improve particle discrimination and energy reconstruction. Finally, extending this approach to a broader range of particle types and more complex event topologies, including overlapping showers and higher detector occupancy scenarios, would be valuable for applications in future high-energy physics experiments.

6. Contributions & Acknowledgements

Liangyu Wu conducted background research on calorimetry techniques and machine learning applications in high-energy physics, performed detector simulations, created the dataset, implemented the neural network architecture, conducted training, performed result analysis and drafted the project report. Qihua Wang contributed to background research on existing methodologies, assisted with model refinement and hyperparameter optimization and performed result analysis and refinement of the report. Bo Liu participated in background research on calorimetry techniques and existing machine learning approaches, and contributed to the interpretation of experimental results and refinement of the report. We would like to thank the TTU team for their development of the Geant4-based detector simulation code that was essential for this project.

References

[1] S. Agostinelli, J. Allison, K. Amako, J. Apostolakis, H. Araujo, P. Arce, M. Asai, D. Axen, S. Banerjee, G. Barrand, F. Behner, L. Bellagamba, J. Boudreau, L. Broglia, A. Brunengo, H. Burkhardt, S. Chauvie, J. Chuma, R. Chytracek, G. Cooperman, G. Cosmo, P. Degtyarenko, A. Dell'Acqua, G. Depaola, D. Dietrich, R. Enami, A. Feliciello, C. Ferguson, H. Fesefeldt, G. Folger, F. Foppiano, A. Forti, S. Garelli, S. Giani, R. Giannitrapani, D. Gibin, J. Gómez Cadenas, I. González, G. Gracia Abril, G. Greeniaus, W. Greiner, V. Grichine, A. Grossheim, S. Guatelli, P. Gumplinger, R. Hamatsu, K. Hashimoto, H. Hasui, A. Heikkinen, A. Howard, V. Ivanchenko, A. Johnson, F. Jones, J. Kallenbach, N. Kanaya, M. Kawabata, Y. Kawabata, M. Kawaguti, S. Kelner, P. Kent, A. Kimura, T. Kodama, R. Kokoulin, M. Kossov, H. Kurashige, E. Lamanna, T. Lampén, V. Lara, V. Lefebure, F. Lei, M. Liendl, W. Lockman, F. Longo, S. Magni, M. Maire, E. Medernach, K. Minamimoto, P. Mora de Freitas, Y. Morita, K. Murakami, M. Nagamatu, R. Nartallo, P. Nieminen, T. Nishimura, K. Ohtsubo, M. Okamura, S. O'Neale, Y. Oohata, K. Paech, J. Perl, A. Pfeiffer, M. Pia, F. Ranjard, A. Rybin, S. Sadilov, E. Di Salvo, G. Santin, T. Sasaki, N. Savvas, Y. Sawada, S. Scherer, S. Sei, V. Sirotenko, D. Smith, N. Starkov, H. Stoecker, J. Sulkimo, M. Takahata, S. Tanaka, E. Tcherniaev, E. Safai Tehrani, M. Tropeano, P. Truscott, H. Uno, L. Urban, P. Urban, M. Verderi, A. Walkden, W. Wander, H. Weber, J. Wellisch, T. Wenaus, D. Williams, D. Wright, T. Yamada, H. Yoshida, and D. Zschiesche. Geant4—a simulation toolkit. *Nuclear Instruments and Methods in Physics Research Section A: Accelerators, Spectrometers, Detectors and Associated Equipment*, 506(3):250–303, 2003.

[2] N. Akchurin, C. Cowden, J. Damgov, A. Hussain, and S. Kunori. On the use of neural networks for energy reconstruction in high-granularity calorimeters. *JINST*, 16(12):P12036, 2021.

[3] A. Aurisano, A. Radovic, D. Rocco, A. Himmel, M. D. Messier, E. Niner, G. Pawloski, F. Psihas, A. Sousa, and P. Vahle. A Convolutional Neural Network Neutrino Event Classifier. *JINST*, 11(09):P09001, 2016.

[4] P. Baldi, K. Cranmer, T. Faucett, P. Sadowski, and D. Whiteson. Parameterized neural networks for high-energy physics. *Eur. Phys. J. C*, 76(5):235, 2016.

[5] F. Carminati, A. Gheata, G. Khattak, P. Mendez Lorenzo, S. Sharan, and S. Vallecorsa. Three dimensional Generative Adversarial Networks for fast simulation. *J. Phys. Conf. Ser.*, 1085(3):032016, 2018.

[6] S. V. Chekanov, S. Eno, S. Magill, C. Palmer, L. Wu, and M. Y. Aamir. Geant4 simulations of sampling and homogeneous hadronic calorimeters with dual readout for future colliders. *Nucl. Instrum. Meth. A*, 1072:170200, 2025.

[7] I. Diehl, F. Feindt, I.-M. Gregor, K. Hansen, S. Lachnit, D. Rastorguev, S. Spannagel, T. Vanat, and G. Vignola. 4D-tracking with digital SiPMs. *Nucl. Instrum. Meth. A*, 1069:169985, 2024.

[8] S. Eno, L. Wu, M. Y. Aamir, S. V. Chekanov, S. Nabili, and C. Palmer. On the resolution of dual readout calorimeters. 1 2025.

[9] Y. Feng and Aesthete. *TTU-HEP/DREAMSim*. 5 2025.

[10] P. T. Komiske, E. M. Metodiev, and M. D. Schwartz. Deep learning in color: towards automated quark/gluon jet discrimination. *JHEP*, 01:110, 2017.

[11] S. Lee, M. Livan, and R. Wigmans. Dual-readout calorimetry. *Reviews of Modern Physics*, 90(2), Apr. 2018.

[12] R. Milton, S. J. Paul, B. Schmookler, M. Arratia, P. Karande, A. Angerami, F. T. Acosta, and B. Nachman. Design and simulation of a SiPM-on-tile ZDC for the future EIC, and its performance with graph neural networks. *Nucl. Instrum. Meth. A*, 1079:170613, 2025.

[13] C. Neubüser, J. Kieseler, and P. Lujan. Optimising longitudinal and lateral calorimeter granularity for software compensation in hadronic showers using deep neural networks. *Eur. Phys. J. C*, 82(1):92, 2022.

[14] A. Pareti. Dual-readout calorimeter development for future High-Energy Physics Experiments. *PoS*, CORFU2023:019, 2024.

[15] F. Sefkow, A. White, K. Kawagoe, R. Pöschl, and J. Repond. Experimental tests of particle flow calorimetry. *Rev. Mod. Phys.*, 88:015003, Feb 2016.